

SURFACE PRESSURE AND WIND LOAD CHARACTERISTICS ON PRISMS IMMERSED IN A TRANSIENT GUST FRONT FLOW FIELD

Kyle Butler^{*}, Shuyang Cao[†], Yukio Tamura[†], Ahsan Kareem^{*}, Shigehira Ozono[‡]

^{*}NatHaz Modeling Laboratory
University of Notre Dame, Notre Dame, IN 46545, USA
e-mails: kbutler3@nd.edu, kareem@nd.edu

[†]Wind Engineering Research Center
Tokyo Polytechnic University, Kanagawa 243-02, Japan
e-mails: cao@arch.t-kougei.ac.jp, yukio@arch.t-kougei.ac.jp

[‡]Department of Applied Physics, Faculty of Engineering
University of Miyazaki, 889-2192, Japan
e-mail: ozono@phys.miyazaki-u.ac.jp

Keywords: Gust fronts, multiple fan wind tunnel, transient surface pressures.

Abstract: *Thunderstorm generated gust fronts are responsible for various degrees of structural damage in many areas of the world. However, the resulting impact of gust front winds is not fully understood to such a level that their flow kinematics, dynamics and impact on structures can be quantified with some certainty. Gust front winds are transient in nature and have a flow profile which differs significantly from a typical boundary layer flow field. This study focuses on investigating the effects of this flow profile and its transient nature on the aerodynamics of bluff, prismatic bodies. A gust front type flow field is generated using a multiple fan wind tunnel and the resulting surface pressures are captured on a suite of prismatic models, which vary in size in relationship to the oncoming wind profile. The temporal variations in surface pressures are analyzed using traditional time, frequency and time-frequency domain schemes. Results indicate the changing nature of the surface pressure field in time, highlighting both qualitative and quantitative differences between local and area-averaged pressures under a host of flow profiles.*

1 INTRODUCTION

Many severe wind events are not caused by typical boundary layer type winds and associated fluctuating components, but by large scale transient phenomena. Thunderstorms, down-burst outflows and gust fronts constitute various extreme wind events that cause significant damage and result in loss of lives and property, particularly to low or mid-rise buildings, transmission lines, industrial structures and, potentially, long span bridges. Studies have shown that thunderstorm winds are the prevailing design wind speeds for higher recurrence intervals of many locations in the United States (e.g. Twisdale and Vickery 1992), highlighting the need for more fundamental studies of the flow behavior. Thus, new simulation and

modeling techniques are required to capture thunderstorm and gust front characteristics. Some characteristics of these events are, primarily, their respective horizontal wind velocity profiles near the ground surface and their short life span. However, the impacts of such events are not as easily quantified as is the impact of typical synoptic boundary layer flow fields, and little is understood about the true nature of their aerodynamic behavior.

The simulation of downbursts and gust fronts has been attempted through various physical and numerical techniques including impinging jets (e.g. Chay and Letchford 2002), large vortex generators (Sarkar et al. 2006), wall jets (Lin and Savory 2006), and a flat plate at high incidence (Butler and Kareem 2007), along with numerical models aimed at reproducing storm event time histories (e.g. Wood et al. 2001). This work presents the use of a new facility to the study gust front wind loads on structures. As opposed to recreating the entire thunderstorm or downburst structure (ie. a descending core column of air), a more basic approach was undertaken to investigate the broader impacts of the ground level outflow from these events, identifying features in the resulting surface pressure field that distinguish these events from impacts due to synoptic flow systems. In order to accomplish this, a newly designed wind tunnel was employed to isolate the impact of two distinct features of gust front flows: the near ground flow profile shape and the rapid, transient changes. The impact of these conditions were captured on multiple square cross-section, prismatic models, to better understand the basic underlying mechanisms that result from the impact of gust front type flow fields and to compare them with the existing body of research about flows around simple prismatic shapes (e.g. Kareem and Cermak 1984, Lin et. al. 2005). The results presented consider both qualitative and quantitative measures to expose the underlying aerodynamics involved.

Beyond the basic bluff body aerodynamics viewpoint, these experimental results build upon the body of knowledge that is currently being incorporated into a new design framework. The Gust Front Factor (GFF) based approach (Kwon and Kareem 2007) centers around the delineation of the impact of the features commonly associated with gust front type flows. The GFF approach, akin to the gust loading factor approach, provides a framework for the codification of the gust front load effects in building design codes. The factor encapsulates static and dynamic characteristics of gust-front wind effects through their distinguishing features: variation in the vertical velocity profile; dynamic effects induced by the sudden rise in wind speed; non-stationarity of turbulence in gust-front wind; transient aerodynamics. This experimental program attempts to address two of these features: the kinematic effects resulting from the velocity pressure relationship in the profile shape and the transient aerodynamic effects resulting from the rapidly varying flow field.

2 EXPERIMENTAL SETUP

Experiments were carried out in the 3-D multiple-fan wind tunnel constructed at the University of Miyazaki, a description of which is given in Fig. 1a. It is comprised of a series of 99 fans arranged in a grid-like pattern, each individually controlled through separate AC servo-motors. The development of this facility from a 2-D to 3-D domain and subsequent experiments utilizing this facility have shown its efficacy in generating and reproducing various statistical characteristics of atmospheric flows (e.g. Nishi and Miyagi 1995, Cao et al. 2001, 2002, Ozono et al. 2006). The test section measures 15.5m long (adjustable), 2.6m wide and 1.8m high. Based on the dynamic nature of this system, and its inherent capability to tailor flow fields, it was presented as an ideal choice to aid in the modeling of gust front type outflows.

In this study, emphasis was placed on generating a transient variation of the mean flow profile while also replicating the general shape of a gust front outflow for detailed surface pres-

sure measurements. The objective was to capture various trends in the pressure response of a prismatic cylinder to both the inflow profile shape and the concurrent increase in flow speed. Surface pressures were monitored on three prismatic models (a general layout of the measurement locations is shown in Fig. 1b) and each varied in height with respect to the height of the level of maximum outflow in the gust profile. The first model (M1) was designed such that the roof level was above the height of the maximum outflow, and contained 176 pressure measurement locations distributed over the windward, side and leeward surfaces. The second prismatic model (M2) was designed such that its height was closest to the level of maximum outflow, and the third prismatic model (M3) was reduced such that its roof level height was below the level of maximum outflow. On each model, pressure measurements were taken at various levels, with 20 pressure measurement locations evenly distributed on each level. Therefore, the smallest model had 60 pressure measurement locations and the mid-height model had 120 measurement locations.

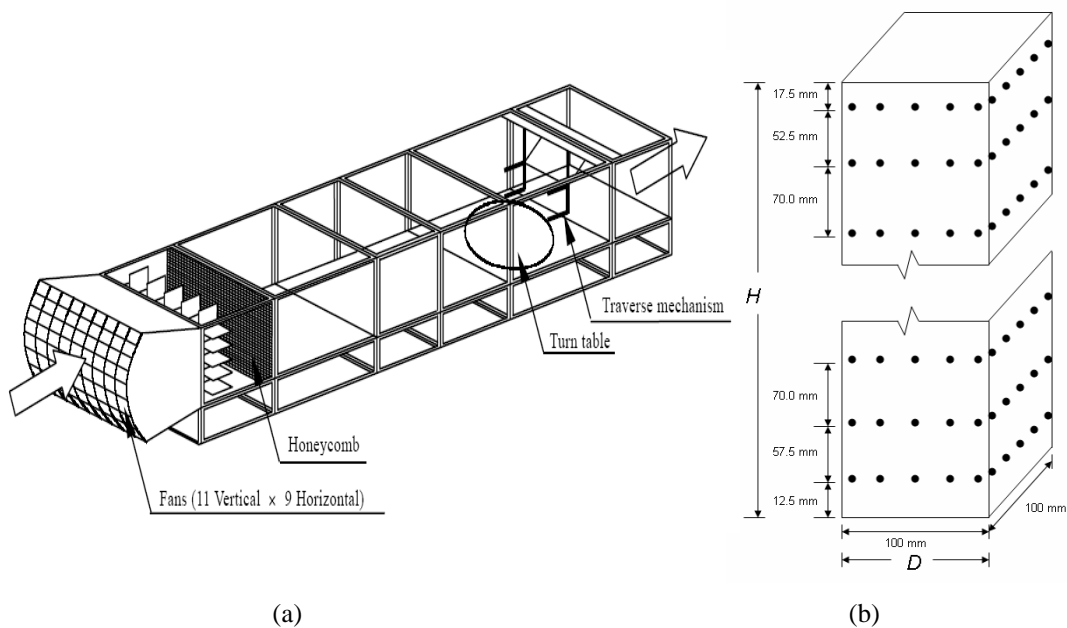


Figure 1: a) Multiple fan wind tunnel setup (Cao et al. 2002) and b) a general schematic of pressure measurement locations on prismatic model.

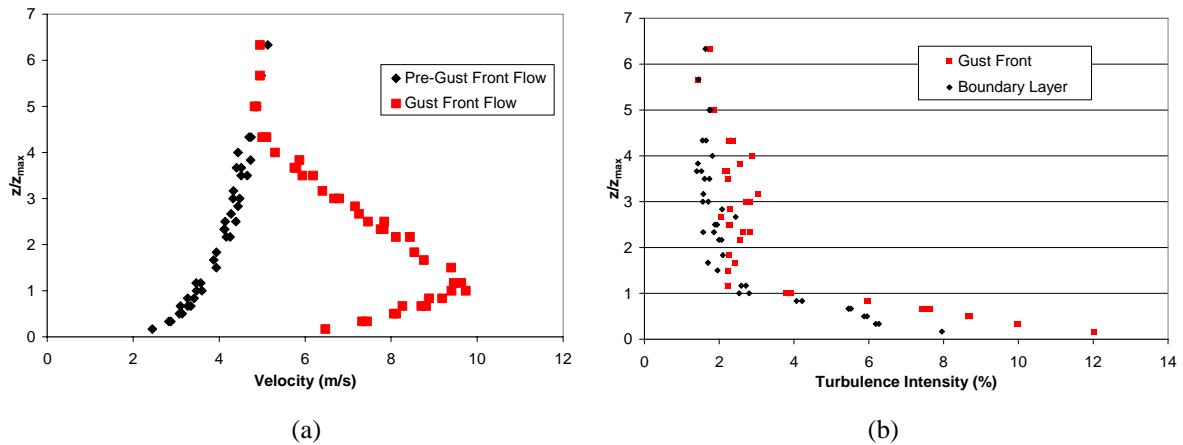


Figure 2: a) Velocity profile of the initial boundary layer flow and the subsequent gust front outflow and b) the turbulence intensity profile of both the boundary layer and gust front flows.

In each test case presented, the velocity variation at the height of maximum outflow between the boundary layer condition and the gust front condition remained fixed and was approximately 7m/s. Each model was subjected to the same, repeated time history of flow conditions and the angle of attack of each model was varied between 0° and 45° . The mean flow profile and the turbulence intensity profiles of both the boundary layer and gust front flow conditions are presented in Fig. 2a and 2b, where z is the height above the surface and z_{max} is the height at which the maximum velocity occurs.

Statistics for the mean profile and turbulence intensity were assessed in the time periods before and after the flow acceleration/deceleration, thus the transient segment is not included. The mean gust front outflow exhibits the characteristic “nose” shape in the near ground region and matches the existing flow regime at the boundary layer height, one of the methods of velocity assessment presented in the GFF framework. The higher turbulence intensity values occur within the region of the increasing flow gradients near ground, while only a slight increase is evident above the maximum outflow. Although there are measurements of turbulence intensity profiles in relation to impinging jets and wall jets (i.e. Chay and Letchford 2002, Lin and Savory 2006), used within a similar context, and through some full scale captures of gust fronts and downbursts (e.g. Orwig and Schroeder 2007), there is little information regarding the full behavior of the gust front profile from which to draw accurate comparisons, particularly regarding the turbulence profile or the transient development of the profile.

3 RESULTS AND DISCUSSION

Each prismatic model studied was exposed to a gust front like event, where the wind speed was accelerated to induce changes in the flow profile that recreated the profile generated from full scale investigations. In this case, the prismatic models were exposed to a boundary layer flow field before a gust front like profile was induced for approximately 80 seconds ending with the wind speed profile given in the initial flow condition, i.e. the boundary layer flow profile. Fig. 3a shows an example time history of the velocity at the maximum outflow level.

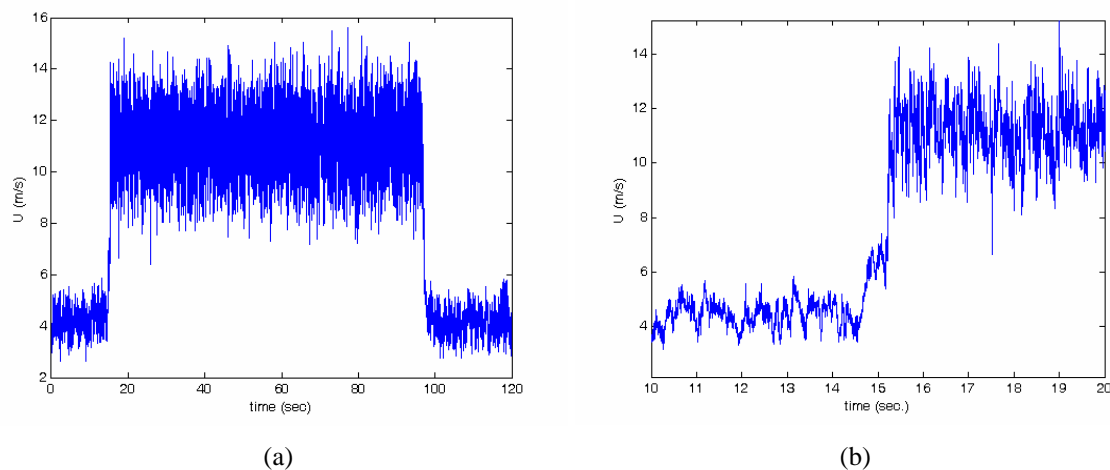


Figure 3: a) Example time history of velocity at maximum outflow and b) cutaway of initial velocity increase.

The scaling of extreme gust events can be based on any number of parameters, e.g. downburst outflow radius or maximum velocity height. In this particular case, the gust scale must be based on the profile shape and the length of the event occurrence. Fujita catalogued various different downburst cases, which can provide a basis for scaling experimental conditions. The downburst profiles examined by Fujita (1985, 1990) identified maximum outflow velocity heights between 30m and 100m and maximum speeds up to approximately 75m/s. Based

on this particular full scale information, length scales linked to the height of maximum outflow produced in the wind tunnel approximately range between 1/120 and 1/400. Velocity scales based on a maximum outflow speed of 11m/s is approximately 1/7, yielding a range of time scales between 1/17 and 1/57. Assuming gust events occur over an interval of 1s to 2s, as presented in this study (a sample time history of which is shown in Fig. 3b, along with a pressure response in Fig. 4b), this represents extreme events lasting 20s to 120s. For comparison, the classic Andrews Air Force Base event in 1983 experienced an increase in velocity from the ambient condition to maximum gust speed occurred within a window of approximately two minutes. However, continued analysis of gust front events will certainly introduce new scaling challenges.

Comparisons of the mean surface pressures within each of the two flow profiles showed variations in both the level of pressure increase and regions of dominant impact. The results for the boundary layer case compare well with other experimental data for tall and low-rise structures (e.g. Surry and Djakovich 1995, Tamura et al. 1997). The mean pressure coefficient on the windward surface of M1, shown in Fig. 4a, indicates a shift in the location of the maximum pressure and an increase in pressures, compared to the initial boundary layer flow, in the lower region of the model surface (where z is the vertical direction, x is the horizontal direction and H and D are the height and width of the model, respectively). In the boundary layer flow, the mean pressure coefficients on the side faces were more negative than that experienced in the gust front flow. Similar trends were also observed on the leeward surface. This may indicate a more coherent flow field around the prism surface, considering there was no significant change in the turbulence intensity above the maximum outflow level. Mean pressures on the low and mid-rise structures behaved in much the same fashion as they do around the taller model. Pressure coefficients on the leeward surface were more negative in the boundary layer flow when compared to the gust flow regime over the entirety of the surface, indicating possible suppressed vortex development that generally occurs with square cylinders.

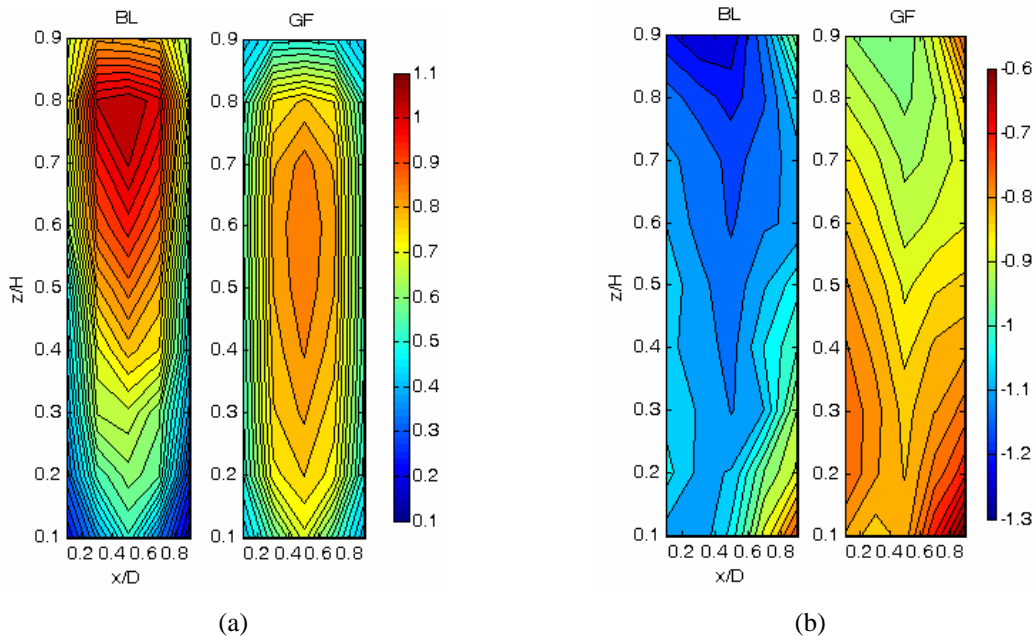


Figure 4: Contours of the mean pressure coefficient on model M1 on (a) windward and (b) side face in both boundary layer (right) and gust front (left) outflows.

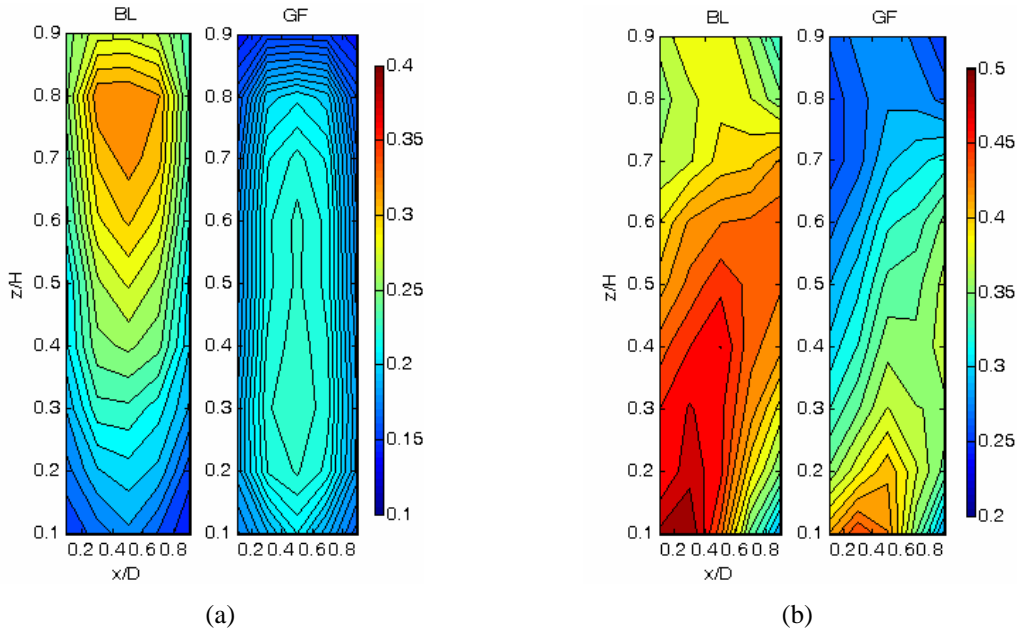


Figure 5: Contours of the RMS of pressure coefficients on model M1 on (a) windward and (b) side face in both boundary layer (right) and gust front (left) outflows.

However, in similar studies regarding gust front flows and their impacts on prismatic models (e.g. Letchford and Chay 2002), it has been identified that the gust event can induce situations where the pressure coefficients achieve an absolute value larger than that given by a quasi-steady estimate. The increase in the pressure coefficients on the side surfaces in the gust flow field, when compared to boundary layer flows for the examined prisms, as well as the concomitant increase in the windward and leeward surfaces, indicates a self-similar nature in the gust front flow profile that exists independently of the approach flow profile.

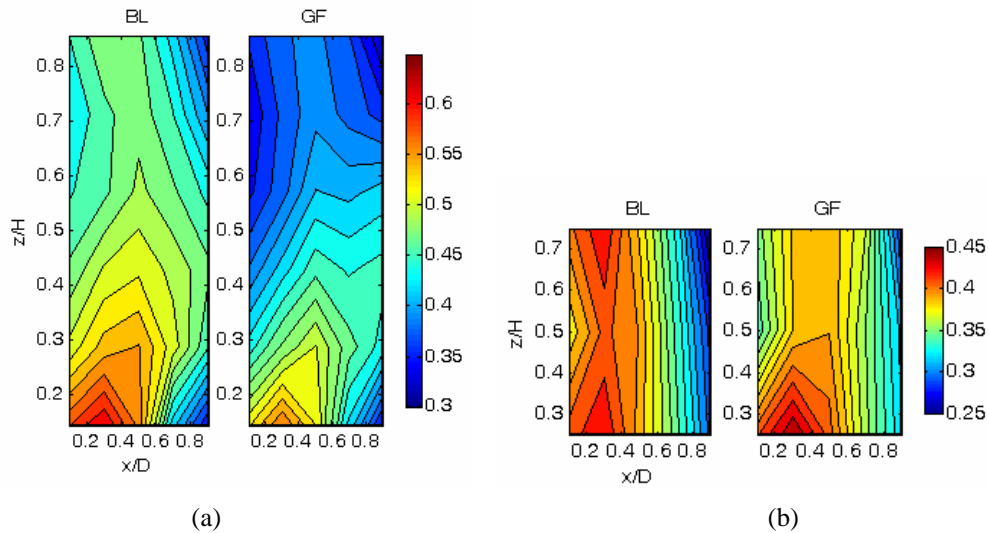


Figure 6: Contours of the RMS of pressure coefficients on the side faces of (a) M2 and (b) M3 in both boundary layer (right) and gust front (left) outflows.

The RMS of the surface pressure fluctuations on M1, shown in Fig. 5b, indicated decreased variability in the pressure coefficient on the side face when the prism was subjected to the gust front flow than compared to the boundary layer flow. Additionally, the variation in pressure coefficient on the mid-rise and low-rise prisms, shown in Fig. 6a and 6b respectively, did show similarity in the distribution of the RMS of pressures corresponding with the height of

the model. The roof level of the mid-rise structure is approximately in line with the height of maximum outflow, and results showed that the mid-rise model had higher pressure coefficient fluctuations on the side face than did that of the high and low-rise models. This could be explained as a result of the nature of opposing gradients in the flow field. The high-rise model experiences both flow gradients, the opposition of which could have a moderating effect on fluctuations on the model surface, and could potentially be responsible for the higher correlations experienced on the side faces. The mid-rise model is subject to the near ground surface velocity gradient, and is indirectly influenced by the opposing velocity gradient not impacted by the model surface. On the other hand, the low-rise model is immersed within the lower half of the velocity gradient and is not influenced by the upper half of the gust front gradient, therefore experiencing lower levels of fluctuations.

Apart from the mean distribution resulting from each profile, the pressure coefficient distribution during the velocity increase reveals more about the impact of the flow structure. Fig. 7 shows the maximum, or minimum, pressure coefficient during the period of accelerated velocity. The windward surface (Fig. 7a) of prism M1 shows two distinct regions of increasing pressure resulting from the dual gradient, while a region of decreasing pressure appears on the trailing edge of the side surface (Fig. 7b) at the height of maximum outflow velocity in the gust profile. The distribution of extreme pressures is altered by the changing flow field, primarily the large velocity gradients which modify the aerodynamics of the surrounding flow.

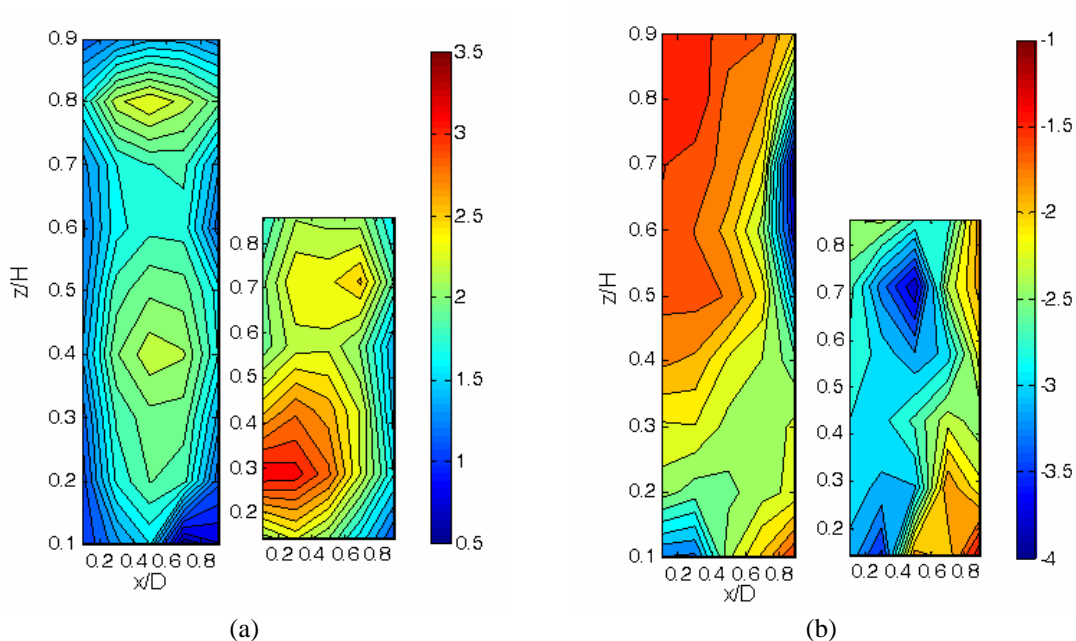


Figure 7: Contours of the instantaneous maximum / minimum pressure coefficients on the (a) windward and (b) side surfaces of M1 and M2 during the velocity rise period.

Correlations of pressures in the chordwise and spanwise directions reveal distinctions regarding both the prism height and inflow profile shape. The spanwise correlation taken at the leading edge (Fig. 8a) indicates that the gust front outflow decreases the level of correlation over the height of the structures, though the level of which is dictated by the prism height. Correlation measures taken along the trailing edge (Fig. 8b) when compared to those taken on the leading edge, show that the subsistence of correlation measures in the gust front flow do not occur, as values decrease more rapidly for prism M1 when compared to the smaller prisms. It is interesting to note, however, when moving from leading edge to trailing edge, that spanwise correlations for the mid and low-rise prisms show that the values for the gust front flow become larger than those of the boundary layer flow at the trailing edge. The

marked difference in the correlations of M1 over the height is indicative of the differing velocity gradients that are experienced.

Similar plots of the chordwise correlation taken at mid-level height, shown in Fig. 9a, on each model prism shows higher correlations for the gust front profile, compared to the boundary layer profile, for M1 than for M2 or M3, where the gust profile correlations are lower. This again may indicate that the large scale flow structure is more coherent within the gust front flow field. Additionally, the spanwise correlation of the profiles along the center line of the windward surface shows that the gust flow profile has a negative correlation in the lower portion of the profile, indicating an opposing flow structure derived from the dual gradients in the flow profile.

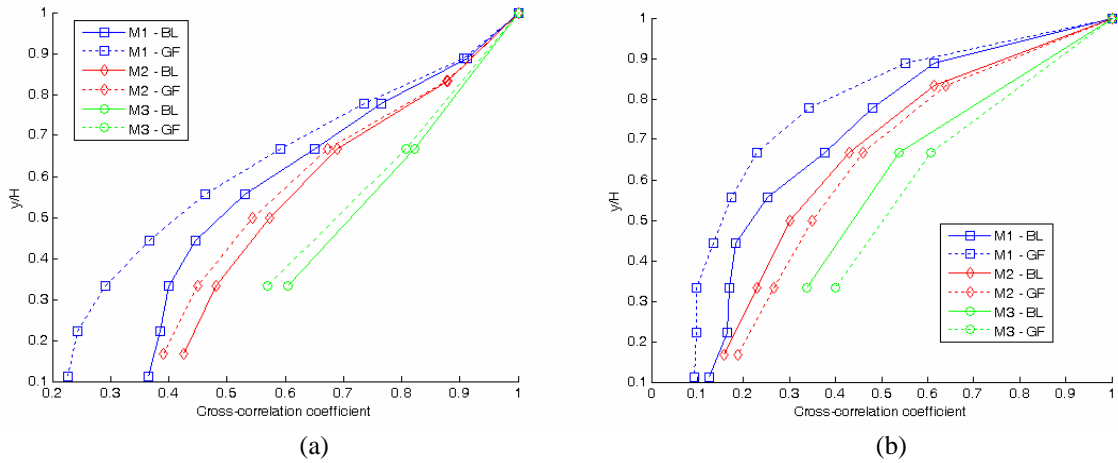


Figure 8: Correlations in the (a) spanwise direction along the leading edge and (b) in the spanwise direction along the trailing edge on prism side face.

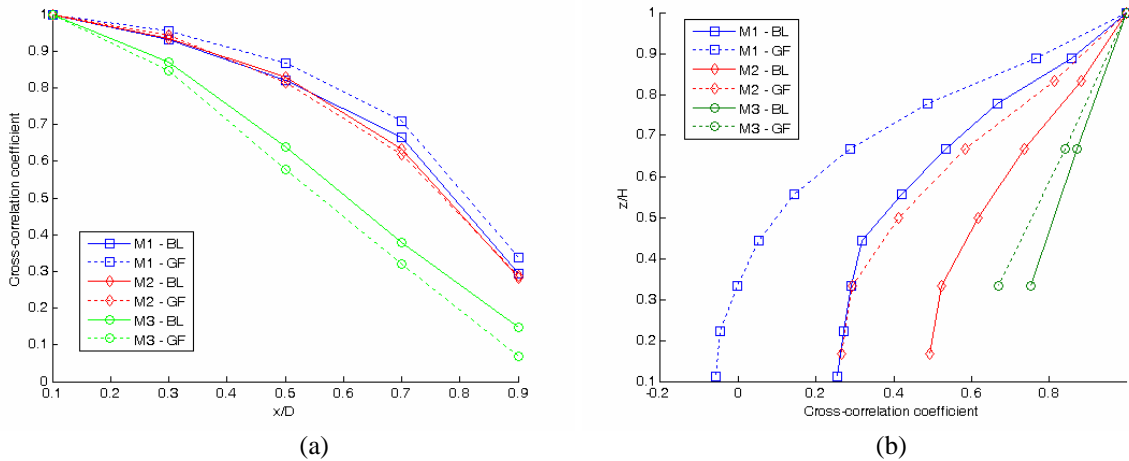


Figure 9: Correlations of pressures taken in the (a) chordwise at mid level height and (b) spanwise along the center line of the windward surface.

Other statistical features, such as the power spectral density (PSD), showed variation in the frequency content at individual pressure measurement locations as result of the changing flow velocity. What is of interest is how the height of the building modifies the frequency component of the resulting flow field as a result of the gust front profile. In similar studies (Butler and Kareem 2007), the effect of turbulence had a spatial evolution with observations from the windward to side face at the leading corner. As mentioned earlier, the height wise dual gradient nature of the flow field has the potential of inducing dual natured effects within the sur-

face pressure regime developed by the existing boundary layer flow. The PSD at mid-level height in the high-rise model, making observations from the leading edge to the trailing edge, shows a peaked nature that becomes more defined with the increasing velocity. There is no shift in the non-dimensional frequency, possibly indicating that the gust front flow profile does not directly change the vortex development around the prism, but that it may be a transient factor.

Comparing the frequency profile of the high-rise structure with that of the mid-rise structure, it is observed that the frequency content changes in much the same manner, though with less relative energy. In addition, the low-rise model has markedly less energy than the taller two models in either flow regime, as development of any stable flow structure is muted with the truncated prism length.

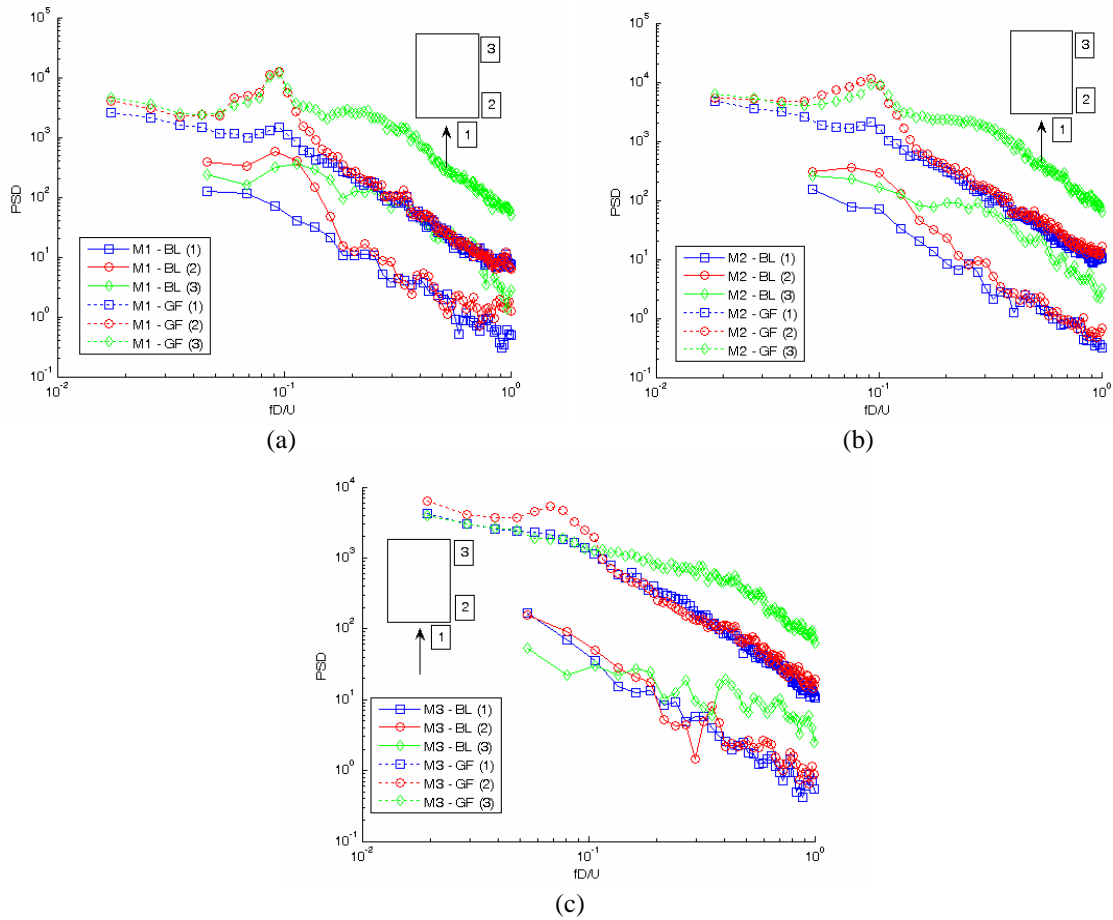


Figure 10: PSD of mid-level pressure measurements on the leading edge and side face for (a) M1, (b) M2 and (c) M3.

Examination of global forces, such as lift and drag, offer more intriguing results. The drag and lift force coefficient generated by the tallest prismatic model, a time history of which is shown in Fig.11a and 12a respectively, reveals no obvious impact in the intensity of either drag or lift due to the changing inflow field. A probability distribution for each force component shows normally distributed lift and a positively skewed distribution for drag. The time history of drag shows a slightly higher shift in the mean value for the boundary layer flow condition, indicating that the gust inflow profile potentially moderates the level of suction on the leeward surface, as well as the level of spanwise vortex formation.

The corresponding wavelet scalograms for the drag and lift time history, shown in Fig. 11b and 12b respectively, reveals frequency content changes, primarily as a result of the changing flow speed. What is interesting to note is that the intensity of the wavelet scalogram for the lift force coefficient decreases once exposed to the gust front profile flow, compared to the boundary layer flow at the beginning and end of each experimental run. Since the intensity of fluctuating lift was not impacted by the changing flow profile, though the wavelet intensity was comparatively reduced, it is estimated that a broader range of frequencies was introduced with the gust front profile. Additionally, there is no identifiable frequency content in the scalogram at the instant of flow acceleration or deceleration, possibly due to the inability of the surrounding flow field to instantaneously adapt to the change in velocity and profile shape.

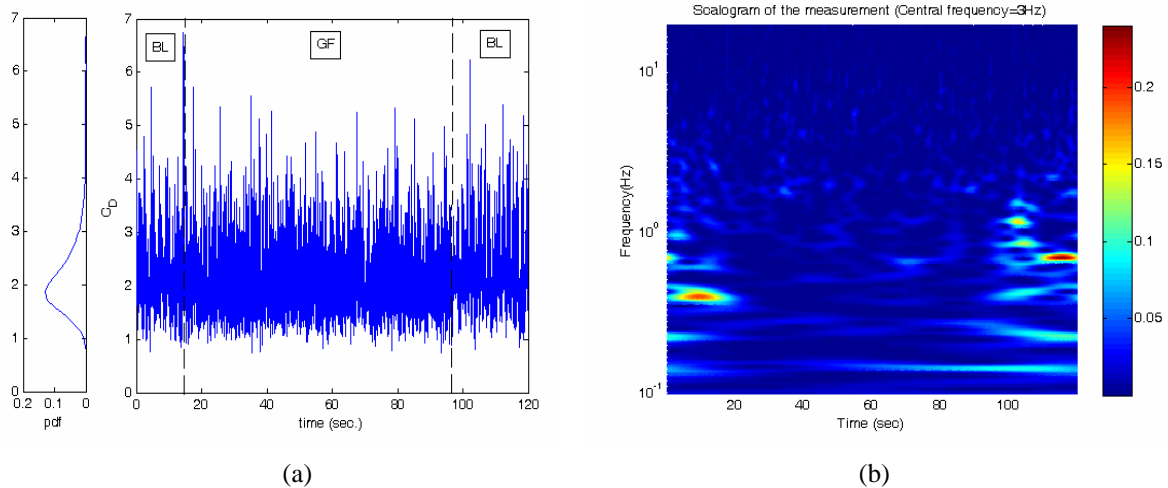


Figure 11: (a) Time history of the drag coefficient for M1 and (b) corresponding wavelet scalogram.

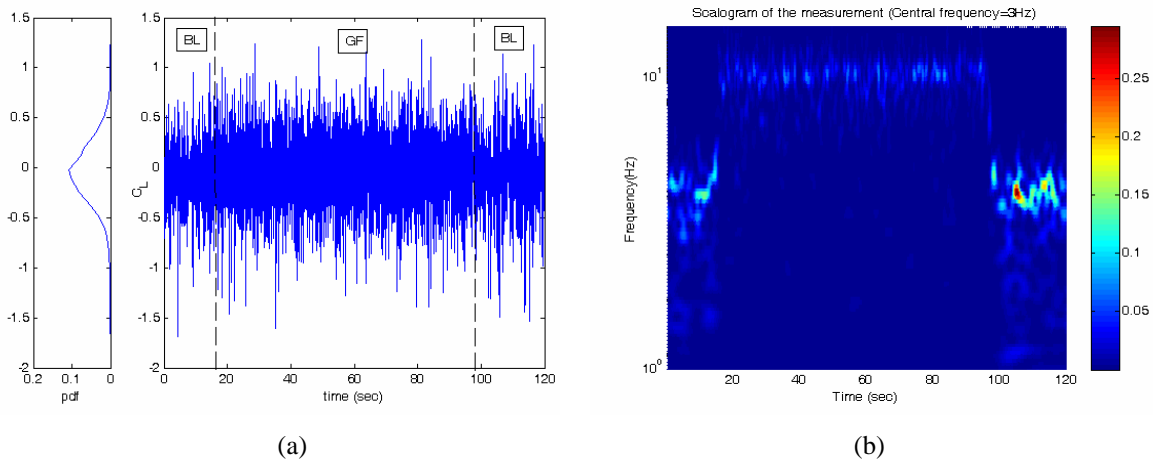


Figure 12: (a) Time history of the lift coefficient for M1 and (b) corresponding wavelet scalogram

Comparing wavelet scalograms for the resulting forces on various prisms, there is a particular trend that becomes apparent in two instances. In both the case of resulting drag and lift behaviors, the occurrence of dominant wavelet scalogram energies occurs before and after the boundary layer flow profile is shifted to the gust flow profile shape. It is worth noting that the turbulence intensity of the gust front inflow profile above the maximum outflow level remains at similar levels, while exhibiting an increase below this level for the gust front flow. It is possible that the turbulence encountered by the model at the lower heights, below the maximum outflow, may impact the level of organized structure development needed for stable vor-

tex shedding over the prism length and the sustenance of frequency contents during the gust front profile flow.

In order to understand the impact of a non-stationary process, different techniques are required beyond traditional stationary analysis schemes. A short-time correlation analysis was performed to uncover the short time behavior of the system. Fig. 13 shows the correlation between two pressure measurement locations on the side face at mid-level height (13a) and the correlation between the oncoming flow and a pressure measurement on the leeward surface (13b). Higher correlation coefficients occurred during the instances of accelerated/decelerated flow. By comparing global attributes, such as lift, and local features, it is apparent that the gust front flow field induces higher correlation of pressures around the model surfaces during significant flow changes, and that the changed flow field also reduced the global pressure impact. Expanding from this, the higher global correlations during the velocity acceleration may attribute to the fact that there are no major frequency contributions during this exchange.

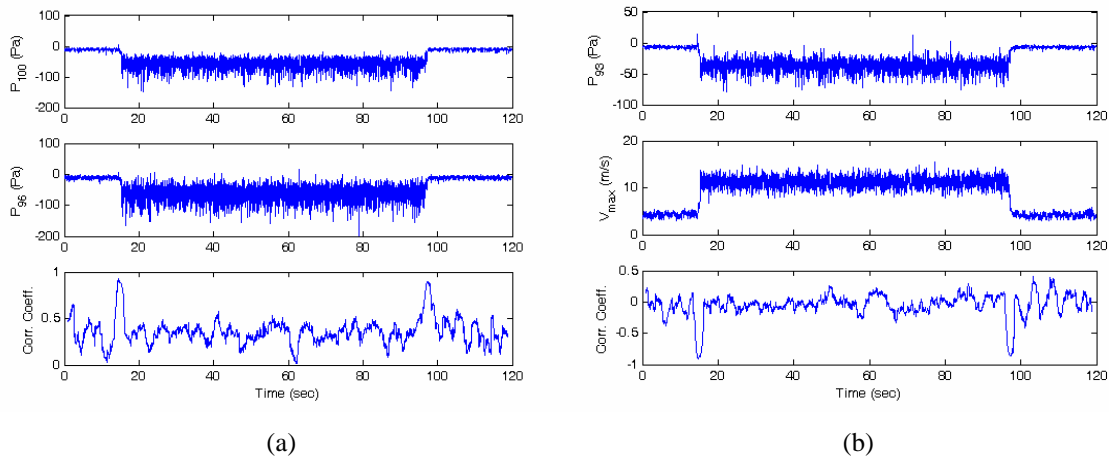


Figure 13: Correlation of a) surface pressures along the side face at mid-level height and b) between the oncoming flow and rear surface pressures.

From global trends to temporally localized behavior, wavelets can again prove useful in uncovering instantaneous behavioral trends in an event. Early research on impulsive flows around circular cylinders (Sarpkaya 1966) showed evidence of a peak in the drag force estimate above the steady state level after the initiation of a transient event, while more recent work has highlighted changes in the drag force frequency content (Matsumoto et al. 2007) for rectangular prisms as well. Fig. 14a and 14b shows zoomed wavelet scalograms of the drag and lift force coefficients respectively, within a 10 second window around the instant of the velocity increase in the gust front flow field occurring on prism M1. In the zoomed wavelet scalogram of the lift coefficient, Fig. 14b, over the velocity increase event, it is noted that the frequency tends to change with the increase in speed, as shown in the time history in Fig. 3a, and this occurs in both the pre and post-gust front events. However, the corresponding drag force coefficient wavelet scalogram, Fig. 14a, shows a brief appearance of two peaks in frequency, similar to that indicated in Fig. 14c observed by Matsumoto et al. 2007, occurring just after the velocity change has reached its steady state level. It was concluded that such a shift was the result of a brief change in the vortex development process (Sarpkaya 1966), though the extent of those changes may be muted in this case considering that there was a pre-existing flow which established a stable vortex development regime and it can be further influenced by other turbulence variations primarily resulting from the dual gradient profile. The

higher intensity content of frequency in the boundary layer flow field compared to the gust front field does suggest that stable vortex development is dependent upon the approach flow topology.

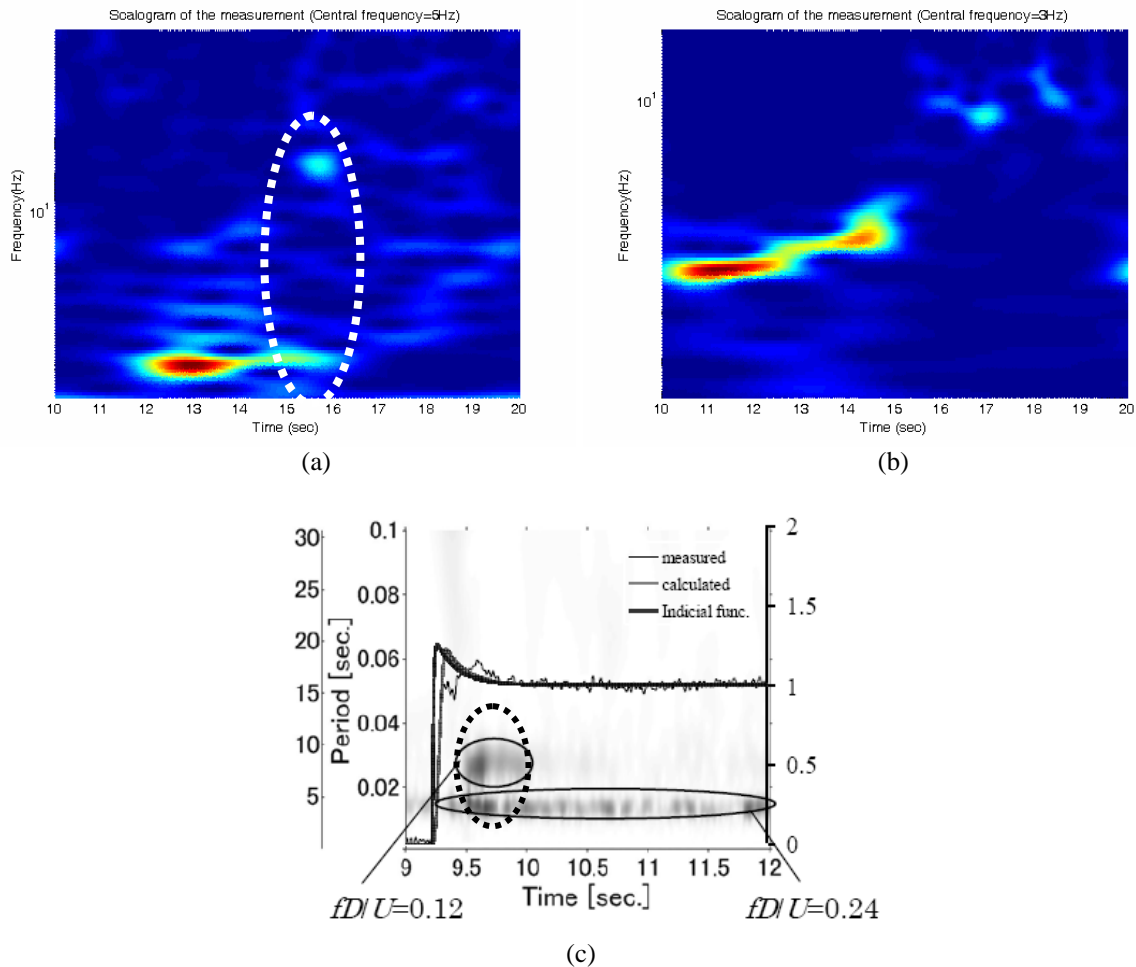


Figure 14: Temporally localized wavelet scalograms of (a) drag force coefficient, (b) lift force coefficient at the instant of gust velocity increase and (c) wavelet scalogram for drag force on a prismatic cylinder with $B/D = 1.0$ (Matsumoto et al. 2007).

For angles of attack beyond 15° , there is little information that can be derived from the frequency domain. As in the case of boundary layer flow (Butler and Kareem 2007), angles of attack beyond approximately 30° have the effect of diminishing the spectral content of the shedding frequency. As shown in Fig. 15, the frequency content for the lift force coefficient is dramatically shifted once the prismatic model is oriented beyond a 0° incidence. There are spectral peaks that remain for the 15° incidence angle, while no dominant frequency component occurs at 30° and 45° incidence.

Assessment of the larger scale flow structure was investigated through the use of co-spectral analysis. The co-spectra between pressure measurement locations on M1 in both the spanwise and chordwise directions were examined. Fig. 16a shows the normalized co-spectra between measurement locations along the leading edge of the side face in the spanwise direction during exposure to the boundary layer type profile. Fig. 16b shows similar information for measurement locations exposed to the gust front flow field. In both cases, the dominant frequency content exists nearest the presumed Strouhal value for the prism. Although conventional co-spectral analysis does not portray the time dependence of embedded correlations

in the pressure field, it is interesting to note that the co-spectral content during exposure to the gust front flow shows more focused content at the Strouhal value when compared to the same content resulting from the boundary layer flow field.

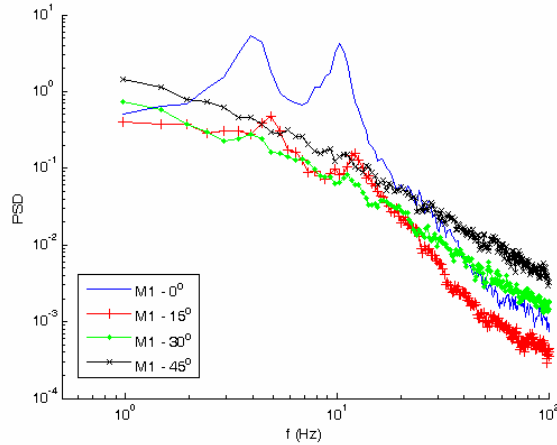


Figure 15: PSD of the lift force coefficient for prism M1 at varying angles of attack.

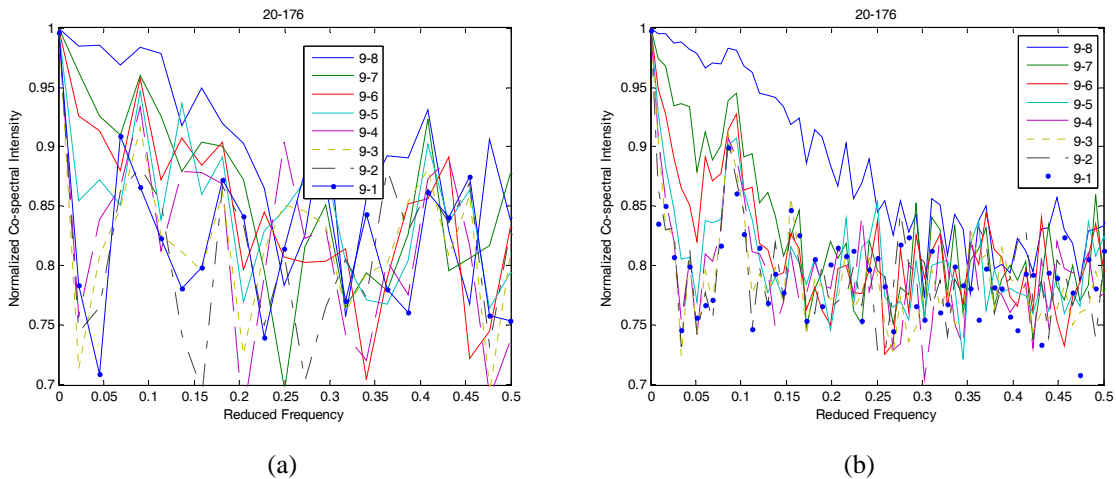


Figure 16: Co-spectra of pressure measurement locations in the spanwise direction along the leading edge due to exposure to the (a) boundary layer flow field and (b) gust front flow field.

Wavelets, similar to those used to examine drag and lift coefficients, were also used to investigate local variations in the dominant frequency content of pressures in time. In this analysis, wavelets were used to examine changes in fluctuating surface pressure frequency. Wavelet co-scalograms were used to identify common frequency content between pressure measurement locations as a function of time, and as a function of the pressure measurement location varying in downstream distance along the side face, at various levels. Fig. 17a shows the wavelet co-spectra for two adjacent pressure locations on the side face (separated by 2 cm.), in the chordwise direction, at midlevel starting at the leading edge. Higher intensity bursts occur intermittently throughout the duration of the gust front profile exposure, and these bursts occur through a range of frequencies with dominant peaks centered on the same frequency as that noted in the lift force, observed in Figure 12b. Similarly, Figure 17b shows a similar wavelet co-spectra between pressure locations at the leading and trailing edge (separated by 8 cm.) on the side face. In this case, the intermittent bursts of frequency occur at the same dominant frequency as noted in Figure 17a, with slightly less intensity in other frequency ranges. It is interesting to note that given the level of velocity fluctuations during the

gust front event, compared to that at the beginning and end of the time series, there are prominent similarities in the frequency content of surface pressures even with an increase in the separation between the points examined. However, there is more intense frequency content when observing the resultant forces, lift force in this case, within the lower velocity flow events before and after the gust front. This observation highlights the peculiarities between the integral pressure fluctuations and the global force, which are being further examined to better understand the interaction of gust front flow topology with the prismatic shape.

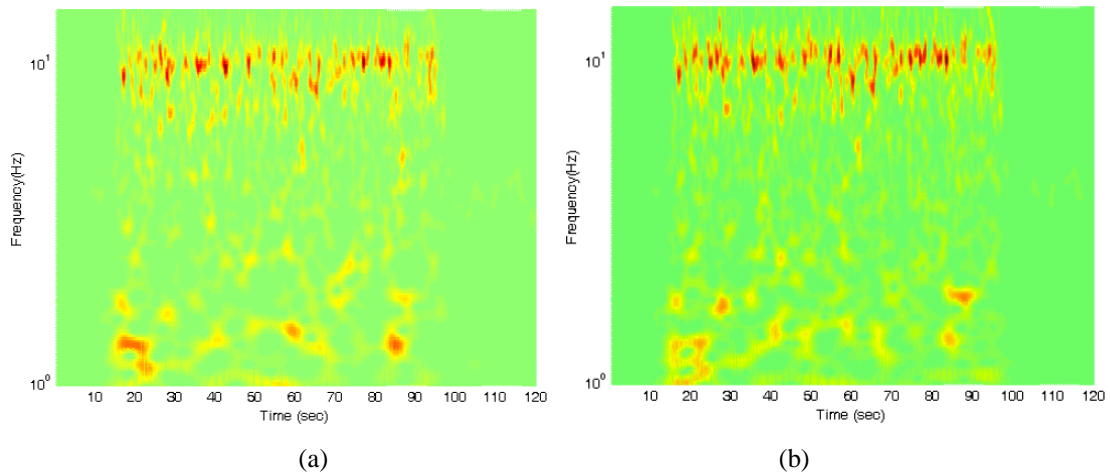


Figure 17: Wavlet Co-scalograms between pressure measurement locations at mid-level height with x/d separation of a) 0.2 and b) 0.8 (with central frequency of 3Hz in both cases).

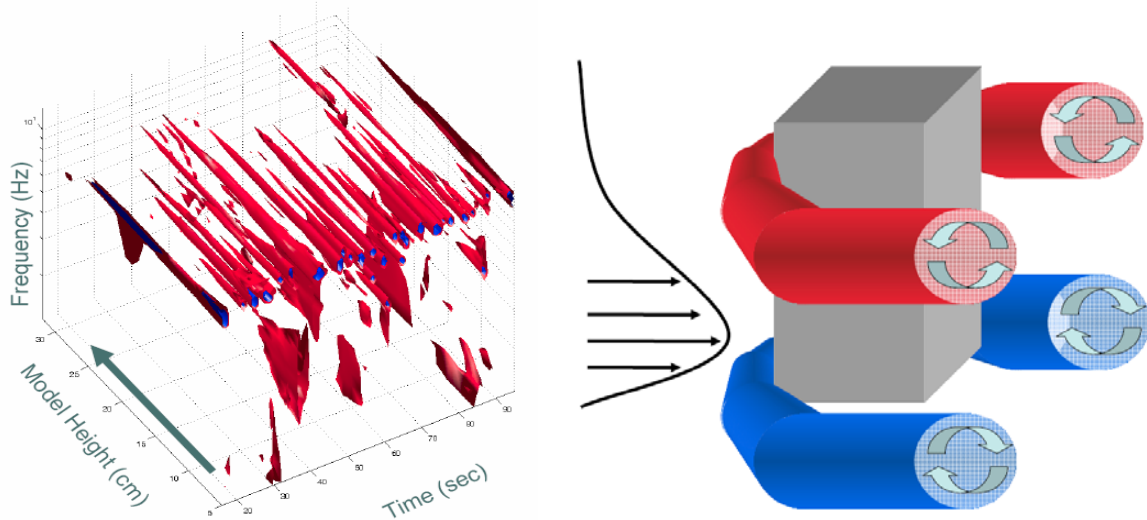


Figure 18: a) 3-dimensional wavelet scalogram generated in the spanwise direction along the leading edge and b) caricature of idealized flow structure resulting from gust front flow.

To assess the nature of the time-frequency variations in surface pressure within a spatial context, scalograms were analyzed at critical points, such as leading and trailing edge corners. Data was organized using a 3-dimensional representation of the wavelet scalogram, where the scalogram was generated for each surface measurement in the spanwise direction and interpolated connections between corresponding values of intensity were drawn. Fig. 18a demonstrates the multi-dimensional wavelet scalogram along with a caricature of gust front type flow field as it wraps around a prism. This allowed for a spatial view of the scalogram energy, to uncover where and when particular frequency contents appeared or ceased to exist.

This representation is aimed at examining the wavelet scalograms to uncover possible transient flow structures, as indicated in Fig. 18b, such as zones of flow separation and rotation where horseshoe type vortices, typical of near surface flows, develop as a pair of contra-rotating vortices possibly as a result of double flow gradients in the oncoming profile. During exposure to the gust flow profile, intermittent high frequency pressure zones, associated with the increased velocity, at the leading edge appear over much of the prism height, while brief low frequency regions appear over the lower height levels. The dual vortex structure may be identified through these low frequency zones, and further refinement of the wavelet scaling could reveal the corresponding zones at the higher levels. This multi-level wavelet scalogram may serve as a critical tool to delineate transient spatio-temporal structures in the pressure field.

4 CONCLUSIONS

A fundamental study aimed at delineating the kinematic and transient effects of variations within the boundary layer flow field on the surface pressures of prismatic models is presented. A multiple fan wind tunnel was employed to simulate a transient gust front flow field with changing flow profile shape. Surface pressures were examined on a suite of prismatic models, capturing transient changes within the flow field. The results of this experiment were examined through traditional statistical methods, and more recent analysis techniques that involve time-frequency domain realizations. It was noted that the correlation of surface pressure around the model surfaces was markedly higher during the flow field acceleration, and the surface pressures extremes revealed characteristics driven by the dual flow profile gradients, compared to the synoptic boundary layer flows before and after, while wavelet scalograms showed marked differences between the typical boundary layer flow field and the gust front profile. Further analysis of these experiments will continue mapping the effects of the gust front flow on the surrounding flow field within a spatio-temporal context.

ACKNOWLEDGEMENTS

The authors would like to thank University of Miyazaki and the Center of Excellence: Wind Effects in Urban Areas and the Global Center of Excellence: New Frontier of Education and Research in Wind Engineering at the Tokyo Polytechnic University for participating in this collaborative effort, as well as NSF Grant CMS 03-24331.

REFERENCES

- [1] L. Twisdale, P. Vickery, Research on thunderstorm wind design parameters, *Journal of Wind Engineering and Industrial Aerodynamics*, 41 (1992) 545-556.
- [2] M. Chay, C. Letchford, Pressure distributions on a cube in a simulated thunderstorm downburst – Part A: stationary downburst observations, *Journal of Wind Engineering and Industrial Aerodynamics*, 90 (2002) 711-732.
- [3] P. Sarkar, F. Haan, V. Balaramudu, A. Sengupta, Laboratory simulation of tornado and microburst to assess wind loads on buildings, *ASCE Structures Congress*, May 17th-19th, 2006, St. Louis, MO, USA.
- [4] W. Lin, E. Savory, Large-scale quasi-steady modeling of a downburst outflow using a slot jet, *Wind and Structures*, 9 (2006) 419-440.
- [5] K. Butler, A. Kareem, Physical and numerical modeling of downburst generated gust fronts, *Proc. 12th International Conference on Wind Engineering*, Cairns, Australia, July 1-6, 2007.

- [6] G. Wood, K. C. S. Kwok, N. Motteram, D. Fletcher, Physical and numerical modeling of thunderstorm downbursts, *Journal of Wind Engineering and Industrial Aerodynamics*, 89 (2001) 535-552.
- [7] A. Kareem, J. Cermak, Pressure fluctuations on a square building model in boundary-layer flows, *Journal of Wind Engineering and Industrial Aerodynamics*, 36 (1990) 589-599.
- [8] N. Lin, C. Letchford, Y. Tamura, B. Liang, O. Nakamura, Characteristics of wind forces acting on tall buildings, *Journal of Wind Engineering and Industrial Aerodynamics*, 93 (2005) 217-242.
- [9] D. Surry, D. Djakovich, Fluctuating pressure on models of tall buildings, *Journal of Wind Engineering and Industrial Aerodynamics*, 58 (1995) 81-112.
- [10] Y. Tamura, H. Ueda, H. Kikuchi, K. Hibi, S. Suganuma, B. Bienkiewicz, Proper orthogonal decomposition study of approach wind-building pressure correlation, *Journal of Wind Engineering and Industrial Aerodynamics*, 72 (1997) 421-431.
- [11] D. Kwon, A. Kareem, Gust-front factor: A new framework for the analysis of wind load effects in gust-fronts, *Proc. 12th International Conference on Wind Engineering*, Cairns, Australia, July 1-6, 2007.
- [12] A. Nishi, H. Miyagi, Computer-controlled wind tunnel for wind-engineering applications, *Journal of Wind Engineering and Industrial Aerodynamics*, 54/55 (1995) 493-504.
- [13] S. Cao, A. Nishi, K. Hirano, S. Ozono, H. Miyagi, H. Kikugawa, Y. Matsuda, Y. Wakasugi, An actively controlled wind tunnel and its application to the reproduction of the atmospheric boundary layer, *Boundary-Layer Meteorology*, 101 (2001) 61-76.
- [14] S. Cao, A. Nishi, H. Kikugawa, Y. Matsuda, Reproduction of wind velocity history in a multiple fan wind tunnel, *Journal of Wind Engineering and Industrial Aerodynamics*, 90 (2002) 1719-1729.
- [15] S. Ozono, A. Nishi, H. Miyagi, Turbulence generated by a wind tunnel of multi-fan type in uniformly active and quasi-grid modes, *Journal of Wind Engineering and Industrial Aerodynamics*, 94 (2006) 225-240.
- [16] K. Orwig, J. Schroeder, Near-surface wind characteristics of extreme thunderstorm winds, *Journal of Wind Engineering and Industrial Aerodynamics*, 95 (2007) 565-584.
- [17] T. T. Fujita, *The downburst: microburst and macroburst*, University of Chicago Press, Chicago, Illinois, 1985, 122p.
- [18] T. T. Fujita, Downbursts: meteorological features and wind field characteristics, *Journal of Wind Engineering and Industrial Aerodynamics*, 36 (1990) 75-86.
- [19] C. Letchford and M. Chay, Pressure distributions on a cube in a simulated thunderstorm downburst – Part B: moving downburst observations. *Journal of Wind Engineering and Industrial Aerodynamics*, 90 (2002) 733-753.
- [20] T. Sarpkaya, Separated flow about lifting bodies and impulsive flow about cylinders, *AIAA Journal*, 4 (1966) 414-420.
- [21] K. Butler, A. Kareem (2007), Characteristics of pressure and integral loads on prisms in boundary layer flows, *Proc. 12th International Conference on Wind Engineering*, Cairns, Australia, July 1-6, 2007.
- [22] M. Matsumoto, M. Shimamura, T. Meada, H. Shirato, T. Yagi, K. Hori, Y. Kawashima, M. Hashimoto, Drag forces on 2-D cylinders due to sudden increase of wind velocity, *Proc. 12th International Conference on Wind Engineering*, Cairns, Australia, July 1-6, 2007.